MODELING THE EARLY MULTIWAVELENGTH EMISSION IN GRB130427A

N. FRAIJA[1], W. LEE[1] AND P. VERES[2]

[1]Instituto de Astronomía, Universidad Nacional Autónoma de México, Apdo. Postal 70-264, Cd. Universitaria, DF 04510, México and
[2]Center for Space Plasma and Aeronomic Research (CSPAR), University of Alabama in Huntsville, Huntsville, AL 35899, USA
(Dated: January 7, 2016)
Draft version January 7, 2016

ABSTRACT

One of the most powerful gamma-ray bursts, GRB 130427A was swiftly detected from GeV γ-rays to optical wavelengths. In the GeV band, the Large Area Telescope (LAT) on board the Fermi Gamma-Ray Space Telescope observed the highest-energy photon ever recorded of 95 GeV, and a bright peak in the early phase followed by emission temporally extended for more than 20 hours. In the optical band, a bright flash with a magnitude of 7.03 ± 0.03 in the time interval from 9.31 s to 19.31 s after the trigger was reported by RAPTOR in r-band. We study the origin of the GeV γ-ray emission, using the multiwavelength observation detected in X-ray and optical bands. The origin of the temporally extended LAT, X-ray and optical flux is naturally interpreted as synchrotron radiation and the 95-GeV photon and the integral flux upper limits placed by the HAWC observatory are consistent with synchrotron self-Compton from an adiabatic forward shock propagating into the stellar wind of its progenitor. The extreme LAT peak and the bright optical flash are explained through synchrotron self-Compton and synchrotron emission from the reverse shock, respectively, when the ejecta evolves in thick-shell regime and carries a significant magnetic field.

Subject headings: gamma-rays bursts: individual (GRB 130427A) — radiation mechanisms: nonthermal

1. INTRODUCTION

Gamma-ray bursts (GRBs) are the most luminous explosions in the universe. Based on photometric and spectroscopic observations, long GRBs (lGRBs) have usually been associated to the core collapse of massive stars leading to supernovae (CCSNe) of type Ib, Ic or II (Woosley & Bloom 2006; Hjorth & Bloom 2012; Hjorth et al. 2003). In the cosmological scenario, the large isotropic energy release (up to $\sim 10^{55}$ erg), short variability timescale (down to $\sim 10^{-3}$ s), and nonthermal gamma-ray spectra leads to an ultrarelativistic expansion with a large bulk Lorentz factor in the range of $10^2 - 10^3$. In the standard fireball model, the expanding relativistic ejecta interacts with the surrounding medium generating reverse and forward shocks. The long-lasting forward shock (FS) leads to a continuous softening of the afterglow spectrum (Panaitescu 2007; Nakar & Piran 2004), whereas the reverse shock (RS) that propagates into the ejecta gives rise to a strong and short peak. After the peak, no new electrons are injected and the material cools adiabatically, although if the central engine emits slowly-moving material the RS could survive from hours to days (Genet et al. 2007; Uhm & Beloborodov 2007).

Due to its intensity and proximity (z=0.34, Levan et al. (2013)), one of the most energetic bursts, GRB 130427A, was observed in GeV-MeV γ-rays, X-rays and the optical band. GRB 130427A was detected on 2013 April 27 at 07:47:06.42 UTC by the Gamma-ray Burst Monitor (GBM) on board Fermi (von Kienlin 2013) and afterwards by several orbiting satellites and multiple ground-based telescopes (Maselli et al. 2014; Ackermann et al. 2014; Pozanenko et al. 2013). The Large Area Telescope (LAT) observed this burst for ~ 70 ks exhibiting a bright peak at ~ 15 s after the GBM trigger. The optical and LAT emission showed a close correlation during the first 7000 s (Vestrand et al. 2014). In particular, a bright optical flash peaking at 15 s was temporally correlated with the LAT peak.

Some authors have claimed that the multiwavelength afterglow observed in GRB 130427A, from dozens of seconds to days after the GBM trigger, can be modeled as synchrotron emission of relativistic electrons accelerated in the stellar wind of the standard reverse and forward shock (Laskar et al. 2013; Perley et al. 2014; Kouveliotou et al. 2013; Maselli et al. 2014). For instance, the bright optical flash was better fitted by reverse shock emission (Vestrand et al. 2014). Other sets of models have interpreted the temporally extended Fermi-LAT flux through the synchrotron radiation, Compton scattering emission and electromagnetic cascades induced by ultrarelativistic hadrons (Ackermann et al. 2014; Fan et al. 2013; Liu et al. 2013).

Recently, we have presented a leptonic model based on an early stellar-wind afterglow to describe the temporally extended LAT, X-ray and optical fluxes, as well as the brightest peak present in the LAT light curve of GRB 110731A (Fraija 2015). In this paper, we apply this model to explain the multiwavelength afterglow observations of GRB 130427A: the bright LAT peak and optical flash by reverse shock emission and the temporally extended LAT, X-ray and optical fluxes by forward shock emission. The paper is arranged as follows: in Section 2 we give a brief description of GRB 130427A observations; in Section 3 we present a leptonic model based on external shocks (forward and reverse) that evolve adiabatically in a stellar wind with the quantities observed in GRB 130427A; in section 4 we discuss our results, and brief conclusions are given in section 5.

2. GRB 130427A

GRB 130427A triggered the Gamma-ray Burst Monitor (GBM) on board the Fermi satellite at 07:47:06.42 UTC on 2013 April 27 (von Kienlin 2013). Promptly, the Burst Alert Telescope (BAT) on board Swift triggered on the ongoing burst at 07:47:57.51 UTC. The structure of the light curve (LC) revealed by the BAT instrument in the 15- to 350-keV band showed a complex structure with a duration of ~ 20 s. The Swift Ultra Violet Optical Telescope (UVOT) began ob-

servations at ~ 181 s, whereas observations with the Swift X-ray Telescope (XRT) started at ~ 195 s (Maselli et al. 2014). Its exceedingly bright prompt emission was also detected by other satellites (SPI-ACS/INTEGRAL; Pozanenko et al. 2013) AGILE; Verrecchia et al. (2013), Konus-Wind; Golenetskii et al. (2013), NuSTAR; Kouveliotou et al. (2013) RHESSI; Smith et al. (2013)) and multiple ground- and space follow-up facilities (MAXI/GSC; Kawamuro et al. (2013), VLT/X-shooter; Flores et al. (2013)). For instance, optical spectroscopy from Gemini-North found the redshift of the GRB to be z=0.34 (confirmed later by VLT/X-shooter; Flores et al. (2013)), revealing the closeness to Earth (Levan et al. 2013) and the optical/near infrared (NIR) counterpart observed with the Hubble Space Telescope suggested the association of GRB 130427A with a Type Ic supernova (SN2013cq) (Levan et al. 2013; Xu et al. 2013). RAPTOR (Rapid Telescope for Optical Response) reported on the bright optical flash with a magnitude of 7.03 ± 0.03 in the time interval from 9.31 s to 19.31 s after the GBM trigger (Vestrand et al. 2014). After the peak, the flash faded with a power law flux decay with index $\alpha = -1.67 \pm 0.07$ and was detected for ~ 80 s until it faded below the $\sim$ 10th magnitude sensitivity limit of the RAPTOR full-sky monitors. LAT followed-up this burst until it became occulted by the Earth 715 s after the GBM trigger. The burst emerged at 3.1 ks and was detected for ~ 20 hr, only interrupted by further occultations (Ackermann et al. 2014). This burst presented the highest fluence with isotropic energy $\sim 1.4 \times 10^{54}$ erg and the highest energy photons ever detected, 73 GeV and 95 GeV observed at 19 s and 244 s, respectively. For a single power-law fit to the energy flux light curve, the Fermi Collaboration reported a temporal index of -1.17 ± 0.06, consistent with other Fermi-LAT bursts (Ackermann et al. 2013). Finally, TeV γ-ray observatories such as the High Altitude Water Cherenkov observatory (HAWC; Lennarz & Taboada (2013); Abeysekara et al. (2015)) and the Very Energetic Radiation Imaging Telescope Array System (VERITAS; Aliu et al. (2014)) followed up observations. Although no statistically significant excess of counts was registered by these TeV observatories, upper limits were placed on the emission.

Given some similarities, such as the presence of a temporally LAT extended emission longer than the duration of the prompt emission and a bright LAT peak in coincidence with the prompt phase between the bursts GRB130427 and GRB110931A, we summarize in Table 1 the relevant observational quantities.

Table 1. Observed quantities for GRB110731A and GRB130427A.

Parameter	GRB110731A	GRB130427A
Isotropic Energy ($\times 10^{54}$ erg)	0.76	0.96
Redshift	2.83	0.34
Duration of prompt emission (s)	$\sim 14^a$	$\sim 138^b$
Peak time (s)	~ 5.5	~ 15
Duration of bright peak (s)	~ 1	~ 9
Duration of extended emission (s)	$\sim 10^3$	$> 10^4$
Prompt GeV emission (erg/cm^2)	0.47×10^{-4}	$\sim 10^{-4}$
Highest energy photon (GeV)	3.4 (at $\sim$ 436 s)	95 (at $\sim$ 244 s)
Main references	1	2, 3, 4

Notes.
^{a} Most of energy was released in the first ~ 7 s.
^{b} Most of energy was released in the first ~ 18 s.
References. (1) Ackermann & et al. (2013); (2) Ackermann et al. (2014); (3) Vestrand et al. (2014); (4) Levan et al. (2013).

3. EXTERNAL SHOCK MODEL

As the ultrarelativistic blast wave spreads into the stellar dense wind of the progenitor, it is decelerated leading to forward and reverse shocks. The afterglow dynamics will depend on its mass and in some cases, the emission processes (synchrotron and/or Compton scattering) generated at internal and external shocks which could be simultaneously present in the light curve (Panaitescu 2007; Nakar & Piran 2004; Kobayashi & Zhang 2003; Wu et al. 2003; Mészáros & Rees 1997a). We hereafter use primes (unprimes) to define the quantities in a comoving (observer) frame, the universal constants c=ℏ=1 in natural units and the values of cosmological parameters $H_0 = 71$ km s^{-1} Mpc^{-1}, $\Omega_m = 0.27$, $\Omega_\lambda = 0.73$ (Spergel et al. 2003). The subscripts f and r refer throughout this paper to the FS and RS, respectively and the convention $Q_x = Q/10^x$ will be adopted in c.g.s. units.

3.1. *Forward Shocks*

Afterglow hydrodynamics involves a relativistic blast wave expanding into the medium with density

$$\rho = A_f \, r^{-2} \quad \text{with} \quad A_f = \frac{\dot{M}_w}{4\pi V_w}, \quad (1)$$

where $\dot{M}_w$ is the mass loss rate and V_w is the wind velocity. Requiring the observable quantities: isotropic energy $E = 1.4 \times 10^{54}$ erg (Ackermann et al. 2014), redshift $z = 0.34$ (Levan et al. 2013; Flores et al. 2013), the stellar wind density $A_f = A_{\star,f} (5.0 \times 10^{11})$ g/cm (Chevalier & Li 2000; Laskar et al. 2013; Perley et al. 2014; Kouveliotou et al. 2013), the bulk Lorentz factor $\Gamma_f = \Gamma_{\star,f} 10^2$ and the index of power-law distribution of accelerated electrons $p = 2.2$, we will apply the leptonic model developed in Fraija (2015). The value of this power index was obtained linking the relation of synchrotron flux ($F_\nu \propto t^{-\alpha} \nu^{-\beta}$) with the observed slopes of temporal decays of GeV γ-ray ($\alpha_{GeV} = -1.17 \pm 0.06$; Ackermann et al. (2014)), X-ray ($\alpha_X = -1.29^{+0.02}_{-0.01}$; Maselli et al. (2014)) and optical ($\alpha_{opt} = -1.67 \pm 0.07$; Vestrand et al. (2014)) fluxes. For an ultra relativistic and adiabatic blast wave, the deceleration time is

$$t_{dec} \simeq 674.2 \, \text{s} \left(\frac{1+z}{1.34} \right) \xi_{-0.3}^{-2} E_{54.3} A_{\star,f}^{-1} \Gamma_{\star,f}^{-4}, \quad (2)$$

where the estimated values of ξ for this case are ~ 1 (low energy) and ~ 0.5 (high energy) (Panaitescu & Mészáros 1998; Chevalier & Li 2000).

Synchrotron emission — . Considering that electrons are accelerated to a power-law distribution $N(\gamma_e)d\gamma_e \propto \gamma_e^{-p} d\gamma_e$ and the energy density is equipartitioned to accelerate electrons and to amplify/create the magnetic field through the micro physical parameters $\epsilon_{e,f}$ and $\epsilon_{B,f}$, respectively, the e-minimum Lorentz factor and the magnetic field can be written as

$$\gamma_{e,m,f} = 3.1 \times 10^4 \, \epsilon_{e,f} \, \Gamma_{\star,f}, \quad (3)$$

and

$$B'_f \simeq 6.6 \times 10^3 \, \text{G} \left(\frac{1+z}{1.34} \right)^{1/2} \xi_{-0.3}^{-1} \epsilon_{B,f}^{1/2} \Gamma_{\star,f} E_{54.3}^{-1/2} t_1^{-1/2} A_{\star,f}, \quad (4)$$

respectively. When the expanding relativistic ejecta encounters the stellar wind, it starts to be decelerated, then electrons are firstly heated and after cooled down by synchrotron emission. Comparing the deceleration time scale

(eq. 2) with the cooling $t_{e,syn} \simeq 3m_e/(16\sigma_T)(1+x_f)^{-1}(1+z)\epsilon_{B,f}^{-1}\rho^{-1}\Gamma_f^{-3}\gamma_e^{-1}$ and the acceleration $t_{acc} \simeq \frac{2\pi\,m_e}{q_e}(1+z)\Gamma_f^{-1}B'_f^{-1}\gamma_e$ time scales for synchrotron radiation, then the cooling and maximum Lorentz factors are $\gamma_{e,c,f} = \frac{3m_e\xi^4}{\sigma_T}(1+x_f)^{-1}(1+z)^{-1}\epsilon_{B,f}^{-1}\Gamma_f A_f^{-1}t$ and $\gamma_{e,max,f} \simeq \sqrt{\frac{9\sqrt{2}q_e}{16\pi\sigma_T}}\xi^{1/2}(1+z)^{-1/4}\epsilon_{B,f}^{-1/4}\Gamma_f^{-1/2}E^{1/4}A_f^{-1/2}t^{1/4}$, respectively. Here σ_T is the Thomson cross section, q_e is the elementary charge and the term $(1+x_f)$ is introduced because a once-scattered synchrotron photon generally has energy larger than the electron mass in the rest frame of the second-scattering electrons (Sari & Esin 2001).

Considering the electron Lorentz factors ($\gamma_{e,i,f}^2$ for i=m,c and max) and eqs. (2) and (3), the synchrotron spectral breaks computed through the synchrotron emission $E_{i,f} = \frac{q_e}{m_e}(1+z)^{-1}\Gamma_f B'\gamma_{e,i,f}^2$ can be written as

$$E_{\gamma,\mathrm{a,f}}^{syn} \simeq 2.1\times 10^{-1}\,\mathrm{eV}\left(\frac{1+z}{1.34}\right)^{-2/5}\xi_{-0.3}^{-6/5}\epsilon_{e,f}^{-1}\epsilon_{B,f}^{1/5}A_{\star,f}^{6/5}$$
$$\times E_{54.3}^{-2/5}t_1^{-3/5}$$

$$E_{\gamma,\mathrm{m,f}}^{syn} \simeq 51.7\,\mathrm{MeV}\left(\frac{1+z}{1.34}\right)^{1/2}\xi_{-0.3}^{-3}\epsilon_{e,f}^2\epsilon_{B,f}^{1/2}E_{54.3}^{1/2}t_1^{-3/2}$$

$$E_{\gamma,\mathrm{c,f}}^{syn} \simeq 7.3\times 10^{-6}\,\mathrm{eV}\left(\frac{1+z}{1.34}\right)^{-3/2}\xi_{-0.3}^5(1+x_f)^{-2}\epsilon_{B,f}^{-3/2}$$
$$\times A_{\star,f}^{-2}E_{54.3}^{1/2}t_1^{1/2}$$

$$E_{\gamma,\mathrm{max,f}}^{syn} \simeq 61.9\,\mathrm{GeV}\left(\frac{1+z}{1.34}\right)^{-3/4}\xi_{-0.3}^{-1/2}E_{54.3}^{1/4}A_{\star,f}^{-1/4}t_1^{-1/4}. \quad (5)$$

The synchrotron self-absorption energy $E_{\gamma,\mathrm{a,f}}^{syn}$ was calculated through the absorption coefficient $\alpha_{\epsilon'_\mathrm{a}}$ (Rybicki & Lightman 1986) and the condition $\alpha_{\epsilon'_\mathrm{a}}r/\Gamma = 1$ (Wijers & Galama 1999; Granot et al. 1999). The maximum synchrotron flux $F_{\gamma,\mathrm{max,f}}^{syn} = N_e P_{\nu,max}/4\pi D^2$ given as a function of the peak spectral power $P_{\nu,max} \simeq \sigma_T(m_e/3q_e)(1+z)^{-1}\Gamma_f B'_f$ can be explicitly written as

$$F_{\gamma,\mathrm{max,f}}^{syn} \simeq 7.1\times 10^5\,\mathrm{mJy}\left(\frac{1+z}{1.34}\right)^{3/2}\xi_{-0.3}^{-1}\epsilon_{B,f}^{1/2}A_{\star,f}D_{28}^{-2}$$
$$\times E_{54.3}^{1/2}t_1^{-1/2}, \quad (6)$$

where D is the luminosity distance from the source.

Using the synchrotron spectral breaks (eq. 5) and synchrotron spectra (Sari et al. 1998), the LC in the fast-cooling regime is

$$[F_\nu]^{syn} = \begin{cases} F_{\nu,fl}^{syn}, & E_{\gamma,\mathrm{c,f}}^{syn} < E_\gamma^{syn} < E_{\gamma,\mathrm{m,f}}^{syn}, \\ F_{\nu,fh}^{syn}, & E_{\gamma,\mathrm{m,f}}^{syn} < E_\gamma^{syn} < E_{\gamma,\mathrm{max,f}}^{syn}. \end{cases} \quad (7)$$

where $F_{\nu,fh}^{syn}$ is

$$F_{\nu,fh}^{syn} = 2.8\times 10^{-1}\,\mathrm{mJy}(1+x_f)^{-1}\left(\frac{1+z}{1.34}\right)^{\frac{p+2}{4}}\xi_{-0.3}^{3(1-\frac{p}{2})}$$
$$\times \epsilon_{e,f}^{p-1}\epsilon_{B,f}^{\frac{p-2}{4}}E_{54.3}^{\frac{p+2}{4}}D_{28}^{-2}t_1^{-\frac{3p-2}{4}}\left(\frac{E_{\gamma,\mathrm{f}}^{syn}}{100\,\mathrm{MeV}}\right)^{-\frac{p}{2}}, (8)$$

and $F_{\nu,fl}^{syn}$ is given in Fraija (2015). The LC in the slow-cooling regime is

$$[F_\nu]^{syn} = \begin{cases} F_{\nu,sl}^{syn}, & E_{\gamma,\mathrm{m,f}}^{syn} < E_\gamma^{syn} < E_{\gamma,\mathrm{c,f}}^{syn}, \\ F_{\nu,sh}^{syn}, & E_{\gamma,\mathrm{c,f}}^{syn} < E_\gamma^{syn} < E_{\gamma,\mathrm{max,f}}^{syn}, \end{cases} \quad (9)$$

with $F_{\nu,sh}^{syn}$ and $F_{\nu,sl}^{syn}$ given by

$$F_{\nu,sh}^{syn} = 6.9\times 10^3\,\mathrm{mJy}(1+x_f)^{-1}\left(\frac{1+z}{1.34}\right)^{\frac{p+2}{4}}\xi_{-0.3}^{3(1-\frac{p}{2})}$$
$$\times \epsilon_{e,f}^{p-1}\epsilon_{B,f}^{\frac{p-2}{4}}E_{54.3}^{\frac{p+2}{4}}D_{28}^{-2}t_1^{-\frac{3p-2}{4}}\left(\frac{E_{\gamma,\mathrm{f}}^{syn}}{10\,\mathrm{keV}}\right)^{-\frac{p}{2}}, (10)$$

and

$$F_{\nu,sl}^{syn} \simeq 2.8\times 10^9\,\mathrm{mJy}\left(\frac{1+z}{1.34}\right)^{\frac{p+5}{4}}\xi_{-0.3}^{\frac{(1-3p)}{2}}\epsilon_{e,f}^{p-1}\epsilon_{B,f}^{\frac{p+1}{4}}A_{\star,f}$$
$$\times E_{54.3}^{\frac{p+1}{4}}D_{28}^{-2}t_1^{-\frac{3p-1}{4}}\left(\frac{E_{\gamma,\mathrm{f}}^{syn}}{2\,\mathrm{eV}}\right)^{\frac{1-p}{2}}, \quad (11)$$

respectively. The transition time (t_0^{syn}) from fast- to slow-cooling spectrum is

$$t_0^{syn} = 5.9\times 10^7\,\mathrm{s}\left(\frac{1+z}{1.34}\right)\xi_{-0.3}^{-4}\epsilon_{e,f}\,\epsilon_{B,f}\,A_{\star,f}. \quad (12)$$

SSC emission — Fermi-accelerated electrons can scatter synchrotron photons up to higher energies $E_{\gamma,i}^{ssc} \simeq 2\gamma_{e,i}^2 E_{\gamma,i}^{syn}$. From the synchrotron spectral breaks (eq. 5), the SSC spectral breaks are

$$E_{\gamma,\mathrm{m,f}}^{ssc} \simeq 1.2\times 10^6\,\mathrm{TeV}\left(\frac{1+z}{1.34}\right)\xi_{-0.3}^{-4}\epsilon_{e,f}^4\epsilon_{B,f}^{1/2}$$
$$\times A_{\star,f}^{-1/2}E_{54.3}t_1^{-2}$$

$$E_{\gamma,\mathrm{c,f}}^{ssc} \simeq 7.7\times 10^{-10}\,\mathrm{eV}\left(\frac{1+z}{1.34}\right)^{-3}\xi_{-0.3}^{12}(1+x_f)^{-4}\epsilon_{B,f}^{-7/2}$$
$$\times A_{\star,f}^{-9/2}E_{54.3}t_1^2. \quad (13)$$

From eqs. (1) and (6), the maximum SSC flux $F_{\gamma,\mathrm{max,f}}^{ssc} \simeq (\sigma_T/m_p)r\rho F_{\gamma,\mathrm{max,f}}^{syn}$ can be explicity written as

$$F_{\gamma,\mathrm{max,f}}^{ssc} \simeq 5.8\times 10^5\,\mathrm{mJy}\left(\frac{1+z}{1.34}\right)^2\epsilon_{B,f}^{1/2}A_{\star,f}^{5/2}D_{28}^{-2}t_1^{-1}. (14)$$

In the Klein-Nishina (KN) regime, the emissivity of IC radiation per electron is independent of the electron energy and reduced in comparison with the classical regime, hence the break energy in KN regime is

$$E_{\gamma,\mathrm{f}}^{KN} \simeq 1.5\times 10^{-4}\,\mathrm{GeV}(1+x_f)^{-1}\left(\frac{1+z}{1.34}\right)^{-2}\xi_{-0.3}^4\epsilon_{B,f}^{-1}\Gamma_{\star,f}^2$$
$$\times A_{\star,f}^{-1}t_1. \quad (15)$$

From the SSC break energies (eq. 13) and Compton spectra (Fraija 2015), the LC in the fast- and slow-cooling regime can be written as

$$[F_\nu]^{ssc} \propto \begin{cases} t^0, & E_{\gamma,\mathrm{c,f}}^{ssc} < E_\gamma^{ssc} < E_{\gamma,\mathrm{m,f}}^{ssc}, \\ t^{-p+1}, & E_{\gamma,\mathrm{m,f}}^{ssc} < E_\gamma^{ssc} < E_{\gamma,\mathrm{max,f}}^{ssc}, \end{cases} \quad (16)$$

and

$$[F_\nu]^{ssc} \propto \begin{cases} t^{-p}, & E_{\gamma,\mathrm{m,f}}^{ssc} < E_\gamma^{ssc} < E_{\gamma,\mathrm{c,f}}^{ssc}, \\ t^{-p+1}, & E_{\gamma,\mathrm{c,f}}^{ssc} < E_\gamma^{ssc} < E_{\gamma,\mathrm{max,f}}^{ssc}, \end{cases} \quad (17)$$

respectively.

3.2. *Reverse Shocks*

For the RS, a simple analytic solution can be derived taking two limiting cases, thick- and thin-shell case, (Sari & Piran 1995) by using a critical Lorentz factor (Γ_c) which is defined by

$$\Gamma_c \simeq 134.1 \left(\frac{1+z}{1.34}\right)^{1/4} \xi_{-0.3}^{-1/2} A_{\star,r}^{-1/4} E_{54.3}^{1/4} T_{90,2}^{-1/4} \, , \quad (18)$$

where T_{90} is the duration of the prompt phase and $A_{\star,r} = A_r/(5.0 \times 10^{11}\,\mathrm{g/cm})$ (Chevalier & Li 2000; Laskar et al. 2013). The synchrotron spectral evolution between RS and FS is related by

$$E_{\gamma,\mathrm{m,r}}^{syn}(t_d) \sim \mathcal{R}_e^2 \mathcal{R}_B^{-1/2} \mathcal{R}_M^{-2} E_{\gamma,\mathrm{m,f}}^{syn}(t_d)$$
$$E_{\gamma,\mathrm{c,r}}^{syn}(t_d) \sim \mathcal{R}_B^{3/2} \mathcal{R}_x^{-2} E_{\gamma,\mathrm{c,f}}^{syn}(t_d)$$
$$F_{\gamma,\mathrm{max,r}}^{syn}(t_d) \sim \mathcal{R}_B^{-1/2} \mathcal{R}_M F_{\gamma,max,f}^{syn}(t_d)\,, \quad (19)$$

where

$$\mathcal{R}_B = \frac{\epsilon_{B,f}}{\epsilon_{B,r}},\ \mathcal{R}_e = \frac{\epsilon_{e,r}}{\epsilon_{e,f}},\ \mathcal{R}_x = \frac{1+x_f}{1+x_r+x_r^2}\ \text{and}\ \mathcal{R}_M = \frac{\Gamma_d^2}{\Gamma_r}, \quad (20)$$

and $\Gamma_d \sim \min(\Gamma_r, 2\Gamma_c)$ is the bulk Lorentz factor at the shock crossing time $t_d \sim \left(\frac{\Gamma_d}{\Gamma_c}\right)^{-4} T_{90}$ and $\Gamma_r = \Gamma_{\star,r} 10^2$ is the bulk Lorentz factor of RS (Zhang et al. 2003; Kobayashi & Zhang 2007). The previous relations tell us that including the re-scaling there is a unified description between forward and reverse shocks, and the distinction between forward and reverse magnetic fields considers that in some central engine models (Usov 1992; Mészáros & Rees 1997b; Wheeler et al. 2000) the fireball could be endowed with '"primordial" magnetic fields. The RS becomes relativistic during its propagation and the ejecta is significantly decelerated. The bulk Lorentz factor at the shock crossing time $t_d \leq T_{90}$ is given by the condition $\Gamma_r > 2\Gamma_c$. Eventually, the shock crossing time could be much shorter than T_{90} depending on the degree of magnetization of the ejecta, defined as the ratio of Poynting flux to matter energy flux $\sigma = L_{pf}/L_{kn} \sim \epsilon_{B,r}$ (Fan et al. 2004b; Zhang & Kobayashi 2005; Kobayashi & Zhang 2007).

Synchrotron emission — . Assuming that electrons are accelerated in the RS to a power-law distribution and the energy density is equipartitioned between electrons and the magnetic field, then the e-minimum Lorentz factor and the magnetic field are

$$\gamma_{\mathrm{e,m,r}} = 116.2 \left(\frac{1+z}{1.34}\right)^{-1/4} \xi_{-0.3}^{1/2} \epsilon_{e,r} \Gamma_{\star,r} A_{\star,r}^{1/4} E_{54.3}^{-1/4} t_{d,1}^{1/4}, \quad (21)$$

and

$$B_r' \simeq 6.6 \times 10^3\,\mathrm{G} \left(\frac{1+z}{1.34}\right)^{1/2} \xi_{-0.3}^{-1} \epsilon_{B,r}^{1/2} \Gamma_{\star,r} E_{54.3}^{-1/2} t_{d,1}^{-1/2}$$
$$\times A_{\star,r}\,, \quad (22)$$

respectively. Comparing the dynamical, cooling and the acceleration time scales as showed for FS, we can obtain the cooling and maximum Lorentz factors. By considering $\gamma_{e,a} \simeq \gamma_{e,m}$ (Sari & Esin 2001) and from eq. (20), we re-scale the synchrotron self-absorption energy between FS and RS as $E_{\gamma,\mathrm{a,r}}^{syn} \sim \mathcal{R}_e^2 \mathcal{R}_B^{-1/5} \mathcal{R}_M^{-2} E_{\gamma,\mathrm{a,f}}^{syn}$. From eqs. (5), (19) and (20),

we get the synchrotron spectral breaks

$$E_{\gamma,\mathrm{a,r}}^{syn} \simeq 1.3 \times 10^{-6}\,\mathrm{eV} \left(\frac{1+z}{1.34}\right)^{-7/5} \xi_{-0.3}^{4/5} \epsilon_{e,r}^{-1} \epsilon_{B,r}^{1/5} \Gamma_{\star,r}^2$$
$$\times A_{\star,r}^{11/5} E_{54.3}^{-7/5} t_{d,1}^{2/5}$$

$$E_{\gamma,\mathrm{m,r}}^{syn} \simeq 1.1 \times 10^2\,\mathrm{eV} \left(\frac{1+z}{1.34}\right)^{-1/2} \xi_{-0.3}^{-1} \epsilon_{e,r}^2 \epsilon_{B,r}^{1/2} \Gamma_{\star,r}^2$$
$$\times A_{\star,r} E_{54.3}^{-1/2} t_{d,1}^{-1/2}$$

$$E_{\gamma,\mathrm{c,r}}^{syn} \simeq 3.7 \times 10^{-8}\,\mathrm{eV} \left(\frac{1+z}{1.34}\right)^{-3/2} \xi_{-0.3}^5 (1+x_r+x_r^2)^{-2}$$
$$\times \epsilon_{B,r}^{-3/2} A_{\star,r}^{-2} E_{54.3}^{1/2} t_{d,1}^{1/2}$$

$$F_{\gamma,\mathrm{max,r}} \simeq 4.1 \times 10^7\,\mathrm{mJy} \left(\frac{1+z}{1.34}\right)^2 \xi_{-0.3}^{-2} \epsilon_{B,r}^{1/2} \Gamma_{\star,r}^{-1} A_{\star,r}^{1/2}$$
$$\times D_{28}^{-2} E_{54.3} t_{d,1}^{-1}\,. \quad (23)$$

Synchrotron LCs are derived in Kobayashi (2000). Relativistic electrons accelerated at RS radiate photons in optical wavelengths. Firstly, synchrotron flux increases proportionally to $\sim t^{1/2}$, being able to reach a peak time at $t_d \sim \left(\frac{\Gamma_d}{\Gamma_c}\right)^{-4} T_{90}$. The optical flux at the peak can be written as

$$F_{\gamma,\mathrm{peak,r}}^{syn} \simeq 1.3 \times 10^5\,\mathrm{mJy} \left(\frac{1+z}{1.34}\right)^{5/4} (1+x_r+x_r^2)^{-1} \xi_{-0.3}^{1/2} \epsilon_{B,r}^{-1/4}$$
$$\times \Gamma_{\star,r}^{-1} A_{\star,r}^{-1/2} D_{28}^{-2} E_{54.3}^{5/4} t_{d,1}^{-3/4} \left(\frac{E_{\gamma,\mathrm{r}}^{syn}}{2\,\mathrm{eV}}\right)^{-1/2}. \quad (24)$$

After that the synchrotron flux starts decreasing as $\sim t^{-3}$ (Kobayashi & Zhang 2003).

SSC emission — . Accelerated electrons can upscatter photons from low to high energies as

$$E_{\gamma,\mathrm{a,r}}^{\mathrm{ssc}} \sim 2\gamma_{e,m,r}^2 E_{\gamma,\mathrm{a,r}}^{syn}, \qquad E_{\gamma,\mathrm{m,r}}^{\mathrm{ssc}} \sim 2\gamma_{e,m,r}^2 E_{\gamma,\mathrm{m,r}}^{syn},$$
$$E_{\gamma,\mathrm{c,r}}^{\mathrm{ssc}} \sim 2\gamma_{e,c,r}^2 E_{\gamma,\mathrm{c,r}}^{syn}, \quad \text{and} \quad F_{\gamma,\mathrm{max,r}}^{\mathrm{ssc}} \sim k\tau F_{\gamma,\mathrm{max,r}}^{syn}, (25)$$

where $k = 4(p-1)/(p-2)$ and $\tau = \frac{\sigma_T N(\gamma_e)}{4\pi r_d}$ is the optical depth of the shell. From eqs. (23) and (25), we get the break SSC energies

$$E_{\gamma,\mathrm{m,r}}^{\mathrm{ssc}} \simeq 2.1 \times 10^3\,\mathrm{MeV} \left(\frac{1+z}{1.34}\right)^{-1} \epsilon_{e,r}^4 \epsilon_{B,r}^{1/2} \Gamma_{\star,r}^4$$
$$\times A_{\star,r}^{3/2} E_{54.3}^{-1},$$

$$E_{\gamma,\mathrm{c,r}}^{\mathrm{ssc}} \simeq 6.5 \times 10^{-8}\,\mathrm{eV} \left(\frac{1+z}{1.34}\right)^{-3/2} \xi_{-0.3}^9 (1+x_r+x_r^2)^{-4}$$
$$\times \epsilon_{B,r}^{-7/2} \Gamma_{\star,r}^{-6} A_{\star,r}^{-6} E_{54.3}^{5/2} t_{d,1}^{1/2},$$

$$F_{\gamma,\mathrm{max,r}}^{\mathrm{ssc}} \simeq 9.3 \times 10^7\,\mathrm{mJy} \left(\frac{1+z}{1.34}\right)^3 \xi_{-0.3}^{-4} \epsilon_{B,r}^{1/2} \Gamma_{\star,r}^{-2} A_{\star,r}^{3/2}$$
$$\times D_{28}^{-2} E_{54.3} t_{d,1}^{-2}, \quad (26)$$

and the break energy at the KN regime is

$$E_{\gamma,r}^{KN} \simeq 4.3 \times 10^{-3}\,\mathrm{GeV} (1+x_r+x_r^2)^{-1} \xi_{-0.3}^2 \epsilon_{B,r}^{-1} E_{54.3} \Gamma_{\star,r}^{-2} A_{\star,r}^{-2}. \quad (27)$$

LC of Compton scattering emission can be analytically derived from Chevalier & Li (2000). For $t < t_d$, we take into account that: i) the maximum synchrotron flux is a constant function of time $F_{\gamma,\mathrm{max}}^{syn} \sim t^0$, ii) the spherical radius

and the number of radiating electrons in the shocked shell region increase with time as $r \sim t$ and $N(\gamma_e) \sim t$, respectively, and iii) the cooling break energy $E_{\gamma,c}^{ssc} \sim \gamma_c^2 E_{\gamma,c}^{syn}$ increases as $\sim t^3$, then the SSC flux increases as $F_\nu^{ssc} \sim E_{\gamma,c}^{ssc\,1/2} F_{\nu,\max}^{ssc} \sim E_{\gamma,c}^{ssc\,1/2} \frac{N_e}{r_d^2} F_{\gamma,\max}^{syn} \sim t^{1/2}$. For $t > t_d$, we consider that the characteristic break energy $E_{\gamma,m}^{ssc} \sim \gamma_m^2 E_{\gamma,m}^{syn}$ decreases as $\sim t^{-1}$, then the SSC flux decreases as $F_\nu^{ssc} \sim E_{\gamma,m}^{ssc\,-(p-1)/2} F_{\nu,\max}^{ssc} \sim E_{\gamma,m}^{ssc\,-\frac{p-1}{2}} \frac{N_e}{r_d^2} F_{\gamma,\max}^{syn} \sim t^{-\frac{p+1}{2}}$. It is worth noting that the decay index of the emission for $t > t_d$ might be higher than $\frac{p-1}{2}$ due to the angular time delay effect (Kobayashi & Zhang 2003). At t_d, the γ-ray flux peaks at (Kobayashi & Zhang 2003):

$$
\begin{aligned}
F_{\gamma,\mathrm{peak,r}}^{ssc} \simeq{}& 6.7 \times 10^{-6} \mathrm{mJy} \left(\frac{1+z}{1.34}\right)^{-1/2} \xi_{-0.3}^9 \, x_r \left(1 + x_r + x_r^2\right)^{-5} \\
& \times \epsilon_{e,r} \, \epsilon_{B,r}^{-7/2} \, \Gamma_{\star,r}^{-6} \, A_{\star,r}^{-6} \, D_{28}^{-2} \, E_{54.3} \, t_{d,1}^{-1/2} \\
& \times \left(\frac{E_{\gamma,r}^{ssc}}{100\,\mathrm{MeV}}\right)^{-1/2}. \qquad (28)
\end{aligned}
$$

4. DISCUSSION

Recently, Fraija (2015) presented a leptonic model based on an early afterglow that evolved in a stellar wind to describe successfully the multiwavelength afterglow observations of GRB110731A. In this work, we have used this model to explain the multiwavelength afterglow observed in GRB 130427A. Requiring the values of isotropic energy $E \simeq 1.4 \times 10^{54}$ erg (Vestrand et al. 2014) and the redshift $z = 0.34 \pm 0.01$ (Levan et al. 2013; Flores et al. 2013), from eq. (2) we have plotted the contour lines of the external medium density and bulk Lorentz factor for five values of the deceleration time $t_{dec} = 10, 15, 20, 50$ and 100 s, as shown in Figure 1. Taking into account the fact that the LAT peak and the bright optical flash were present and also showed a close correlation in the time interval [9.31 s,19.31 s] (Vestrand et al. 2014), we have considered the values of the external medium density and bulk Lorentz factor for which the deceleration time (eq. 2) is $t_{dec}=10$ s (line in black color).
To obtain the values of densities ($A_{\star,f/r}$) and the equipartition parameters ($\epsilon_{B,f/r}$ and $\epsilon_{e,f/r}$) that reproduce the multiwavelength afterglow observed in GRB 130427A, we have used the method of Chi-square χ^2 minimization as implemented in the ROOT software package (Brun & Rademakers 1997). The LAT flux has been fitted by synchrotron radiation from FS and SSC emission from RS; the whole temporally extended emission using synchrotron LC in the fast-cooling regime (eq. 8) and the bright peak at 15 s with SSC emission (eq. 28), for high-energy electrons emitting photons at 100 MeV. The X-ray flux has been fitted with the synchrotron LC in the slow-cooling regime for electrons radiating at $E_{\gamma,f}^{syn} = 10$ keV (eq. 10), and the optical flux has been described by synchrotron radiation from FS and RS; the temporally extended emission using the LC of FS in the slow-cooling regime (eq. 11) and the bright optical flash with the LC of RS in fast-cooling regime (eq. 24) for $E_{\gamma,r}^{syn} = 2$ eV.
Figure 2 (left panel) visualizes the values of equipartition parameters, $\epsilon_{B,f}$ and $\epsilon_{e,f}$ for $A_{\star,f} = 10^{-1}$, that reproduce the temporally extended emissions of LAT, X-ray and optical data (see Figure 3). It displays areas in red, blue and green colors. The area in red exhibits the set of parameters that describes the extended LAT component, the area in blue displays those parameters that describe the X-ray emission and the area in

green the parameters that describe the extended optical flux. Regions where the areas intercept correspond to the set of parameters that reproduces more than one flux at the same time. As shown, the set of parameter values: $\epsilon_{e,f} \sim 0.32$ and $\epsilon_{B,f} \sim 3 \times 10^{-5}$ for $A_{\star,f} = 10^{-1}$ and $\Gamma_{\star,f} \simeq 5.5$, can reproduce the temporally extended LAT, X-ray and optical fluxes. Figure 2 (right panel) visualizes the values of equipartition parameters, $\epsilon_{B,r}$ and $\epsilon_{e,r}$ for $A_{\star,r} = 10^{-1}$, that describe the bright LAT peak and the optical flash (see Figure 3). It shows areas in green and yellow. The area in green exhibits the set of parameters that describes the LAT peak and the area in yellow displays those parameters that explain the bright optical flash. It can be seen that the set of parameter values: $\epsilon_{e,r} \sim 0.32$ and $\epsilon_{B,r} \sim 0.13$ for $A_{\star,r} = 10^{-1}$ and $\Gamma_{\star,r} \simeq 5.5$, is able to generate the bright LAT peak and the optical flash.
Figure 3 shows the contributions of synchrotron radiation from FS (dashed lines) and RS (dotted-dashed line), and SSC (continuous line) emission from RS to the multiwavelength afterglow observed in GRB 130427A.
In Table 2, we summarize the equipartition parameters, densities and bulk Lorentz factors found after fitting the multiwavelength afterglow observed in GRB130427A. In addition, the parameters obtained for GRB 110731A have been included in order to compare them with those obtained in GRB 130427A.

Table 2. Parameters found after fitting the multiwavelength afterglow observations of GRB110731A and GRB130427A.

	GRB110731A	GRB130427A
Forward shock		
$\epsilon_{B,f}$	7×10^{-5}	3×10^{-5}
$\epsilon_{e,f}$	0.4	0.32
A_f $(5 \times 10^{11}$ g/cm$)$	10^{-1}	10^{-1}
Γ_f	520	550
Reverse shock		
$\epsilon_{B,r}$	0.28	0.13
$\epsilon_{e,r}$	0.4	0.32
A_r $(5 \times 10^{11}$ g/cm$)$	10^{-1}	10^{-1}
Γ_r	520	550

The set of parameter values obtained using our model is similar to those used to successfully describe the afterglow observed at different times (Laskar et al. 2013; Perley et al. 2014; Ackermann et al. 2014). Comparing the equipartition parameters in both shocks, it is possible to observe that the energy fraction going into electron acceleration is equal ($\mathcal{R}_e = 1$) and the magnetic fields in both shocks (eqs. 4 and 22) are different $B_r' = \mathcal{R}_B^{-1/2} B_f' = 65.8\, B_f'$.
Putting together the parameters for both GRB130427A and GRB110731A, a strong similarity can be noted between them. For instance, the value of the bulk Lorentz factor found for GRB130427A lies not only in the range of GRB 110731A but also in the similar range of values ($\Gamma \sim 500$ - 600) demanded for most LAT-detected and high-redshift GRBs (Veres & Mészáros 2012).
Using the values of parameters reported in Table 2 and eqs. (9), (13), (23), (26), the observable quantities have been computed, as shown in Table 3. Again, we have put together the observable quantities obtained for GRB 110731A.
The maximum photon energy achieved by synchrotron radiation is $E_{\gamma,\max,f}^{syn} = 107.7$ (60.6) GeV for t=$10\,(10^2)$ s. Therefore, the highest-energy photon of 95 GeV at 244 s after the GBM trigger cannot be generated from synchrotron

radiation in the standard afterglow model. The highest-energy photon could be interpreted in the SSC framework, for which the VHE flux is expected to peak at $\simeq$ 22 TeV (see Table 3). However, high-energy photons were searched for in this burst by the HAWC observatory, and although no significant excess of counts was observed, upper limits were placed (Abeysekara et al. 2015). Figure 4 shows the integral flux upper limits placed by HAWC observatory in the time interval [11.5 - 33 s] and the SSC emission without (continuous line) and with (dashed line) the effect of the EBL absorption (dashed; Franceschini et al. (2008)). As shown, the SSC flux (less than 1 TeV) is low enough to be observed by HAWC when it was running at 10% of the final detector. Therefore, with the parameters found after fitting the multiwavelength afterglow (see table 2) not only the highest-energy photon but also the VHE photon non-detection of GRB 130427A could be interpreted in the SSC framework.

Table 3. Quantities obtained with our model for GRB110731A and GRB130427A

	GRB110731A	GRB130427A
Forward shock		
t_{dec} (s)	5.6	9.9
B'_f (G)	52.7	18.9
Synchrotron emission		
$E_{\gamma,\mathrm{a,f}}^{syn}$ (eV)	5.6×10^{-4}	3.3×10^{-2}
$E_{\gamma,\mathrm{m,f}}^{syn}$ (keV)	77.5	23.1
$E_{\gamma,\mathrm{c,f}}^{syn}$ (eV)	0.30	1.3
$E_{\gamma,\mathrm{max,f}}^{syn}$ (GeV)	36.9	107.7
SSC emission		
$E_{\gamma,\mathrm{m,f}}^{ssc}$ (TeV)	11.7	22.1
$E_{\gamma,\mathrm{c,f}}^{ssc}$ (TeV)	8.4×10^{-8}	1.4×10^{-7}
$E_{\gamma,\mathrm{f}}^{KN}$ (TeV)	42.3×10^{-3}	102.3×10^{-3}
Reverse shock		
Γ_c	472.5	236.7
B'_r (G)	3.8×10^3	1.7×10^3
Synchrotron emission		
$E_{\gamma,\mathrm{a,r}}^{syn}$ (eV)	4.3×10^{-8}	0.5×10^{-7}
$E_{\gamma,\mathrm{m,r}}^{syn}$ (eV)	128.9	14.3
$E_{\gamma,\mathrm{c,r}}^{syn}$ (eV)	0.9×10^{-5}	2.5×10^{-5}
SSC emission		
$E_{\gamma,\mathrm{m,r}}^{ssc}$ (MeV)	1.1×10^2	0.6×10^2
$E_{\gamma,\mathrm{c,r}}^{ssc}$ (eV)	5.9×10^{-3}	1.4×10^{-5}
$E_{\gamma,\mathrm{r}}^{KN}$ (GeV)	52.7	166.2

The values of deceleration time and critical Lorentz factor computed in our model are self-consistent with the fact that both the bright LAT peak and the optical flash take place in the time interval [9.31 s,19.31 s] peaking at 15 s and the RS evolves in the thick-shell case ($\Gamma_r > 2\Gamma_c$).

The synchrotron self-absorption energies from FS and RS are in the weak self-absorption regime, then, as observed in LC of GRB 130427A, there is no thermal peak in the synchrotron spectrum due to pile-up electrons (Kobayashi et al. 2004; Gao et al. 2013a).

Unlike GeV, X-ray and optical early observations, GRB130427A started to be observed at $\sim$ 0.3 days in radio wavelengths. This burst was followed for more than 4 months by Westerbork Synthesis Radio Telescope (WSRT), European Very Long Baseline Interferometry Network (EVN), Combined Array for Research in Millimeter Astron-

omy (CARMA), Very Large Array (VLA) and other radio observatories (van der Horst et al. 2014; Perley et al. 2014). In particular, the observable quantities of radio observations at 15 GHz are given in Table 4 (van der Horst et al. 2014).

Table 4. Temporal power-law indices and fluxes of radio observation at 15 GHz (van der Horst et al. 2014).

Temporal index	Time range (days)	Flux (mJy)
0.33 ± 0.20	0.3 - 0.7	~ 3.6
-1.16 ± 0.14	0.7 - 4	~ 1.1
-0.48 ± 0.07	4 - 60	~ 0.2

Following Gao et al. (2013b), we derive the LC of synchrotron radiation from FS in the radio frequencies. The synchrotron spectrum in the radio frequencies is

$$[F_\nu]^{syn} = F_{\gamma,\mathrm{max,f}}^{syn}$$
$$\times \begin{cases} \left(\frac{E_{\gamma,\mathrm{f}}^{syn}}{E_{\gamma,\mathrm{m,f}}^{syn}} \right)^{1/3} & \text{for } E_{\gamma,\mathrm{a,f}}^{syn} < E_{\gamma,\mathrm{f}}^{syn} < E_{\gamma,\mathrm{m,f}}^{syn} < E_{\gamma,\mathrm{c,f}}^{syn}, \\ \left(\frac{E_{\gamma,\mathrm{f}}^{syn}}{E_{\gamma,\mathrm{m,f}}^{syn}} \right)^{-\frac{p-1}{2}} & \text{for } E_{\gamma,\mathrm{a,f}}^{syn} < E_{\gamma,\mathrm{m,f}}^{syn} < E_{\gamma,\mathrm{f}}^{syn} < E_{\gamma,\mathrm{c,f}}^{syn}. \end{cases} \quad (29)$$

From eqs. (2), (5) and (6), we get that the maximum synchrotron flux and the characteristic break synchrotron energy as a function of time are $F_{\gamma,\mathrm{max,f}}^{syn} \propto \epsilon_{B,f}^{1/2} A_{\star,f}^{3/2} D^{-2} \Gamma_{\star,f}^2$ and $E_{\gamma,\mathrm{m,f}}^{syn} \propto \epsilon_{e,f}^2 \epsilon_{B,f}^{1/2} A_{\star,f}^{1/2} \Gamma_{\star,f}^2 t^{-1}$, respectively. Taking into account the values reported in Table 2 and the synchrotron spectrum (Gao et al. 2013b), the LC of synchrotron radiation in the radio frequencies is in the form

$$[F_\nu]^{syn} = \begin{cases} F_{\nu,rh}^{syn}, & E_{\gamma,\mathrm{a,f}}^{syn} < E_{\gamma,\mathrm{f}}^{syn} < E_{\gamma,\mathrm{m,f}}^{syn} < E_{\gamma,\mathrm{c,f}}^{syn}, \\ F_{\nu,rs}^{syn}, & E_{\gamma,\mathrm{a,f}}^{syn} < E_{\gamma,\mathrm{m,f}}^{syn} < E_{\gamma,\mathrm{f}}^{syn} < E_{\gamma,\mathrm{c,f}}^{syn}, \end{cases} (30)$$

with $F_{\nu,rh}^{syn}$ and $F_{\nu,rs}^{syn}$ given by

$$F_{\nu,rh}^{syn} \sim 2.6\,\mathrm{mJy} \left(\frac{1+z}{1.34} \right) \xi^{2/3} \epsilon_{e,f,0.5}^{-2/3} \epsilon_{B,f,-4.5}^{1/3} A_{\star,f,-1}^{4/3} D_{28}^{-2}$$
$$\times \Gamma_{\star,f,0.2}^{4/3} t_{4.6}^{1/3} \left(\frac{E_{\gamma,\mathrm{f}}^{syn}}{15\,\mathrm{GHz}} \right)^{1/3}, \quad (31)$$

and

$$F_{\nu,rs}^{syn} \sim 0.4\,\mathrm{mJy} \left(\frac{1+z}{1.34} \right) \xi^{p-1} \epsilon_{e,f,0.5}^{p-1} \epsilon_{B,f,-4.5}^{\frac{p+3}{4}} A_{\star,f,-1}^{\frac{p+5}{4}} D_{28}^{-2}$$
$$\times \Gamma_{\star,f,-0.3}^{p+1} t_6^{-\frac{p-1}{2}} \left(\frac{E_{\gamma,\mathrm{f}}^{syn}}{15\,\mathrm{GHz}} \right)^{-\frac{p-1}{2}}, (32)$$

respectively. At $t = 4 \times 10^4$ s, the synchrotron self-absorption and characteristic break energies are $E_{\gamma,\mathrm{a,f}}^{syn} \sim 3.5$ GHz and $E_{\gamma,\mathrm{m,f}}^{syn} \sim 142.4$ GHz, respectively, and at $t = 10^6$ s, these break energies are $E_{\gamma,\mathrm{a,f}}^{syn} \sim 0.5$ GHz and $E_{\gamma,\mathrm{m,f}}^{syn} \sim 1.1$ GHz, respectively, then the transition of flux densities between $F_{\nu,rh}^{syn}$ and $F_{\nu,rs}^{syn}$ occurs at $t_m \sim 10^5$ s. Here, t_m is the critical time when the characteristic break energy crosses the observed energy $E_{\gamma,\mathrm{f}}^{syn} \sim 15$ GHz. Comparing the values given in Table 4 with the temporal power-law indeces and fluxes obtained in eq. (30), for p=2.2 the radio observations provide a consistency check for our early time modeling.

As previously calculated, the magnetic field ratio between the reverse and forward shocks is $\frac{B'_r}{B'_f} \simeq 66$. This result strongly suggests that for GRB 130427A the ejecta must be magnetized, thus altering the temporal and spectral properties in the photon and neutrino spectra (Zhang & Kumar 2013; Fraija 2014; Fan & Wei 2005; Fan et al. 2004a; Jin & Fan 2007; Shao & Dai 2005).

5. CONCLUSIONS

We have applied the leptonic model previously introduced in Fraija (2015) in order to describe the early afterglow emission of GRB 110731A. We have modeled the extended LAT, X-ray and optical emission by synchrotron emission from FS, and the bright LAT peak and optical flash by SSC and synchrotron emission from RS, respectively.

We have considered that the ejecta propagating into the stellar wind is decelerated early, at ~ 10 s and the RS evolves in the thick-shell regime. Taking into account the values for redshift $z = 0.34$, isotropic energy $E \simeq 1.4 \times 10^{54}$ erg and the stellar wind $A_f = 5.0 \times 10^{10}$ g/cm, the value of the bulk Lorentz factor as required for most LAT-detected long-duration gamma-ray bursts lies in the range ($\Gamma \sim 500$ - 600) (Veres & Mészáros 2012; Ackermann & et al. 2013; Ackermann et al. 2014).

To find the values of equipartition parameters $\epsilon_{B,f/r}$ and $\epsilon_{e,f/r}$, we have assumed that the magnetic field and electron parameters are constant and then fittted the multiwavelength afterglow LCs; the extended temporally emissions (LAT, X-ray and optical) by synchrotron radiation from the FS and the bright LAT peak and optical flash by SSC and synchrotron emission from RS, respectively (see fig. 3). The values of the parameters found using our model (see table 2) correspond to those typically used to explain the afterglow observed at different times and energy bands (Laskar et al. 2013; Perley et al. 2014; Ackermann et al. 2014).

The set of parameter values obtained using our model is similar to those used to describe successfully the afterglow observed at different times. Although some authors have claimed that the GeV emission detected by LAT in coincidence with the prompt phase could have an internal origin (Maxham et al. 2011; Zhang et al. 2011; He et al. 2011; Liu & Wang 2011), this is the first time that the bright LAT peak and the optical flash are observed temporally correlated, being the former event successfully interpreted as RS emission in the early afterglow framework (Vestrand et al. 2014). Therefore, it is overwhelming evidence that the bright LAT peak around the afterglow onset time comes from the RS as has been explained in this work.

We have restricted our modeling to the first $\sim 10^3$ s of GRB 130427A when only optical and higher energy observations are available. For this GRB, radio observations started at $\sim 3 \times 10^4$ s. While detailed modeling of the late time emission is outside of the scope of this paper, following Gao et al. (2013b) we derive the LC of synchrotron emission from FS in the radio frequencies and extrapolate our model to $\sim$ GHz at $0.3 \leq t \leq 60$ days (van der Horst et al. 2014). Comparing the temporal indeces and fluxes of the radio observations reported in Table 4 with the values obtained in our model (temporal power-law indeces $\alpha = 0.33$ and -0.6, fluxes ~ 2.6 mJy and 0.4 mJy for $t \lesssim 10^5$ s and $t \gtrsim 10^5$ s, respectively), we show that our model is consistent to explain the radio observations of this burst. It is worth noting that the reverse shock contribution in radio is not significant, that is why we calculate the FS flux.

Since GRB 130427A is the most powerful burst detected with a $z \leq 0.5$, copious target photons are expected for photo-hadronic interactions, making them promising candidates for neutrino detection. Searches for high-energy neutrinos in spatial and temporal coincidence around this burst were performed, although no neutrinos were observed (Blaufuss 2013). As found in this work, the magnetic field in the reverse-shock region is stronger ($\simeq 66$ times) than in the forward-shock region, indicating that the ejecta of GRB 130427A is magnetized. The null neutrino result reported by IceCube Collaboration could be explained in the framework of magnetized outflow where neutrino flux is degraded as was previously pointed out by Zhang & Kumar (2013) and Fraija (2014).

It is worth noting that although any significant excess of counts coming from GRB 130427A has not been observed by the HAWC observatory, nowadays bursts with identical features can be detected by this TeV γ-ray observatory. Hence, similar bursts could bring to light information on external medium density, bulk Lorentz factors and energy fractions converted to accelerate electron and/or amplify magnetic fields, thus potentially further constraining possible models.

REFERENCES

Abeysekara, A. U., Alfaro, R., Alvarez, C., et al. 2015, ApJ, 800, 78
Ackermann, M., & et al. 2013, ApJ, 763, 71
Ackermann, M., Ajello, M., Asano, K., et al. 2013, ApJS, 209, 11
—. 2014, Science, 343, 42
Aliu, E., Aune, T., Barnacka, A., et al. 2014, ApJ, 795, L3
Blaufuss, E. 2013, GRB Coordinates Network, 14520, 1
Brun, R., & Rademakers, F. 1997, Nuclear Instruments and Methods in Physics Research A, 389, 81
Chevalier, R. A., & Li, Z.-Y. 2000, ApJ, 536, 195
Fan, Y. Z., & Wei, D. M. 2005, MNRAS, 364, L42
Fan, Y. Z., Wei, D. M., & Wang, C. F. 2004a, MNRAS, 351, L78
—. 2004b, A&A, 424, 477
Fan, Y.-Z., Tam, P. H. T., Zhang, F.-W., et al. 2013, ApJ, 776, 95
Flores, H., Covino, S., Xu, D., et al. 2013, GRB Coordinates Network, 14491, 1
Fraija, N. 2014, ApJ, 787, 140
—. 2015, ApJ, 804, 105
Franceschini, A., Rodighiero, G., & Vaccari, M. 2008, A&A, 487, 837
Gao, H., Lei, W.-H., Wu, X.-F., & Zhang, B. 2013a, MNRAS, 435, 2520

Gao, H., Lei, W.-H., Zou, Y.-C., Wu, X.-F., & Zhang, B. 2013b, New Astronomy Reviews, 57, 141
Genet, F., Daigne, F., & Mochkovitch, R. 2007, MNRAS, 381, 732
Golenetskii, S., Aptekar, R., Frederiks, D., et al. 2013, GRB Coordinates Network, 14487, 1
Granot, J., Piran, T., & Sari, R. 1999, ApJ, 527, 236
He, H.-N., Wu, X.-F., Toma, K., Wang, X.-Y., & Mészáros, P. 2011, ApJ, 733, 22
Hjorth, J., & Bloom, J. S. 2012, The Gamma-Ray Burst - Supernova Connection, 169–190
Hjorth, J., Sollerman, J., Møller, P., et al. 2003, Nature, 423, 847
Jin, Z. P., & Fan, Y. Z. 2007, MNRAS, 378, 1043
Kawamuro, T., Shidatsu, M., Nakahira, S., et al. 2013, GRB Coordinates Network, 14462, 1
Kobayashi, S. 2000, ApJ, 545, 807
Kobayashi, S., Mészáros, P., & Zhang, B. 2004, ApJ, 601, L13
Kobayashi, S., & Zhang, B. 2003, ApJ, 597, 455
—. 2007, ApJ, 655, 973
Kouveliotou, C., Granot, J., Racusin, J. L., et al. 2013, ApJ, 779, L1
Laskar, T., Berger, E., Zauderer, B. A., et al. 2013, ApJ, 776, 119

Lennarz, D., & Taboada, I. 2013, GRB Coordinates Network, 14549, 1

Levan, A. J., Fruchter, A. S., Graham, J., et al. 2013, GRB Coordinates Network, 14686, 1

Liu, R.-Y., & Wang, X.-Y. 2011, ApJ, 730, 1

Liu, R.-Y., Wang, X.-Y., & Wu, X.-F. 2013, ApJ, 773, L20

Maselli, A., Melandri, A., Nava, L., et al. 2014, Science, 343, 48

Maxham, A., Zhang, B.-B., & Zhang, B. 2011, MNRAS, 415, 77

Mészáros, P., & Rees, M. J. 1997a, ApJ, 476, 232

—. 1997b, ApJ, 482, L29

Nakar, E., & Piran, T. 2004, MNRAS, 353, 647

Panaitescu, A. 2007, MNRAS, 379, 331

Panaitescu, A., & Mészáros, P. 1998, ApJ, 493, L31

Perley, D. A., Cenko, S. B., Corsi, A., et al. 2014, ApJ, 781, 37

Pozanenko, A., Minaev, P., & Volnova, A. 2013, GRB Coordinates Network, 14484, 1

Rybicki, G. B., & Lightman, A. P. 1986, Radiative Processes in Astrophysics

Sari, R., & Esin, A. A. 2001, ApJ, 548, 787

Sari, R., & Piran, T. 1995, ApJ, 455, L143

Sari, R., Piran, T., & Narayan, R. 1998, ApJ, 497, L17

Shao, L., & Dai, Z. G. 2005, ApJ, 633, 1027

Smith, D. M., Csillaghy, A., Hurley, K., et al. 2013, GRB Coordinates Network, 14590, 1

Spergel, D. N., Verde, L., Peiris, H. V., et al. 2003, ApJS, 148, 175

Uhm, Z. L., & Beloborodov, A. M. 2007, ApJ, 665, L93

Usov, V. V. 1992, Nature, 357, 472

van der Horst, A. J., Paragi, Z., de Bruyn, A. G., et al. 2014, MNRAS, 444, 3151

Veres, P., & Mészáros, P. 2012, ApJ, 755, 12

Verrecchia, F., Pittori, C., Giuliani, A., et al. 2013, GRB Coordinates Network, 14515, 1

Vestrand, W. T., Wren, J. A., Panaitescu, A., et al. 2014, Science, 343, 38

von Kienlin, A. 2013, GRB Coordinates Network, 14473, 1

Wheeler, J. C., Yi, I., Höflich, P., & Wang, L. 2000, ApJ, 537, 810

Wijers, R. A. M. J., & Galama, T. J. 1999, ApJ, 523, 177

Woosley, S. E., & Bloom, J. S. 2006, ARA&A, 44, 507

Wu, X. F., Dai, Z. G., Huang, Y. F., & Lu, T. 2003, MNRAS, 342, 1131

Xu, D., de Ugarte Postigo, A., Leloudas, G., et al. 2013, ApJ, 776, 98

Zhang, B., & Kobayashi, S. 2005, ApJ, 628, 315

Zhang, B., Kobayashi, S., & Mészáros, P. 2003, ApJ, 595, 950

Zhang, B., & Kumar, P. 2013, Physical Review Letters, 110, 121101

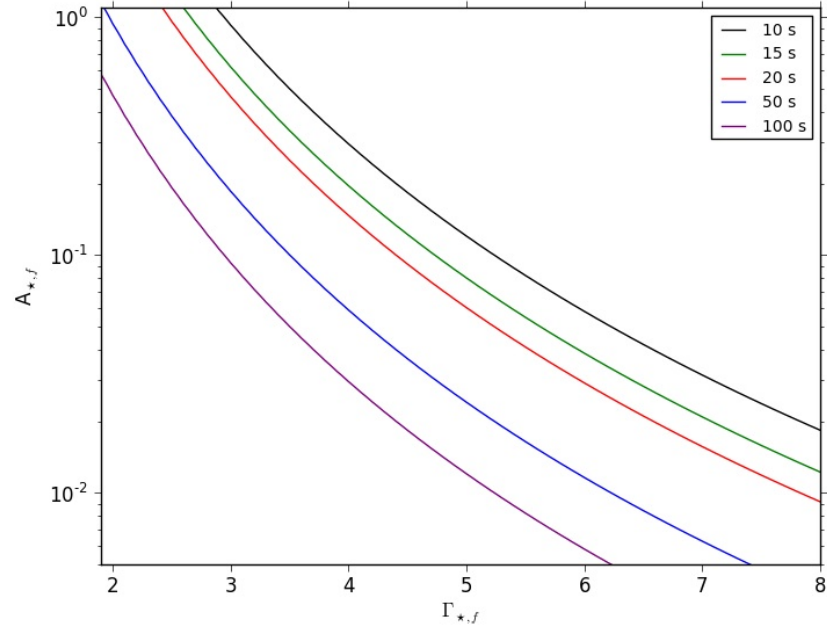Zhang, B.-B., Zhang, B., Liang, E.-W., et al. 2011, ApJ, 730, 141

FIG. 1.— Contour lines of $A_{\star,f}$ and bulk Lorentz factor ($\Gamma_{\star,f}$) as a function of the deceleration time t_{dec}. We use four values of deceleration times $t_{dec} = 10, 15, 20, 50$ and 100 s
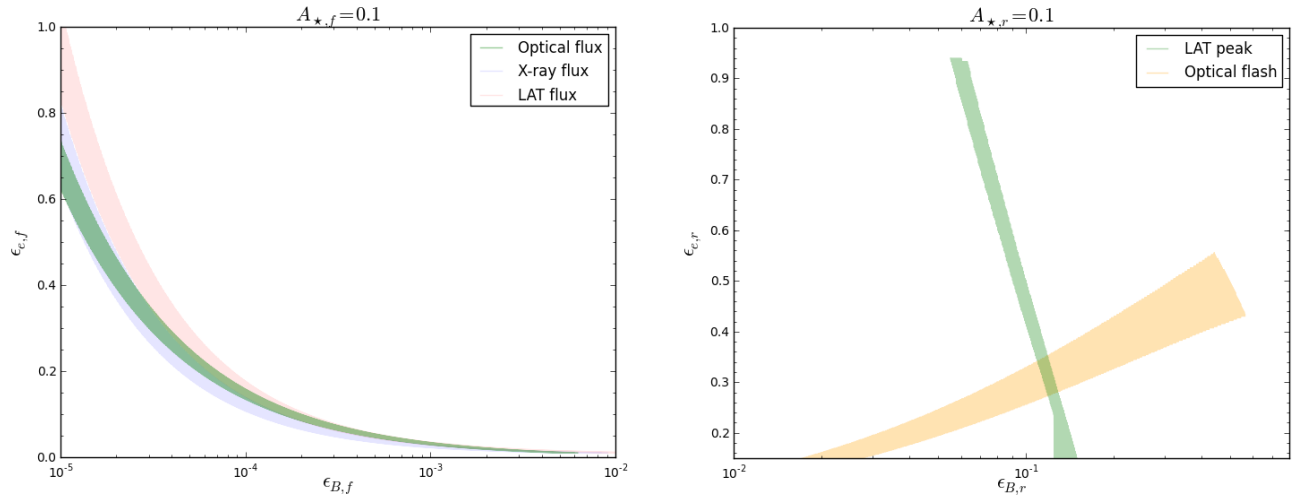

FIG. 2.— Values of equipartition parameters for the FS (right) and RS (left) that reproduce the multiwavelength afterglow observed in GRB 130427A.
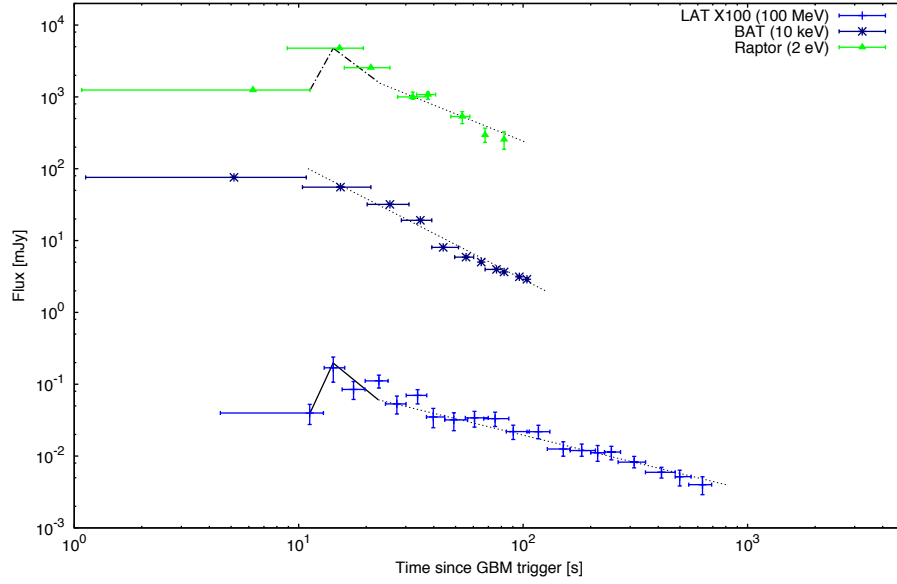
FIG. 3.— Fits of the multiwavelength LCs of GRB 130427A observation with our model. We use the RS in the thick-shell regime to describe the GeV peak (continuous line) and optical flash (dash-dotted line) and the FS to explain the temporally extended LAT, X-ray and optical emissions (dashed lines).
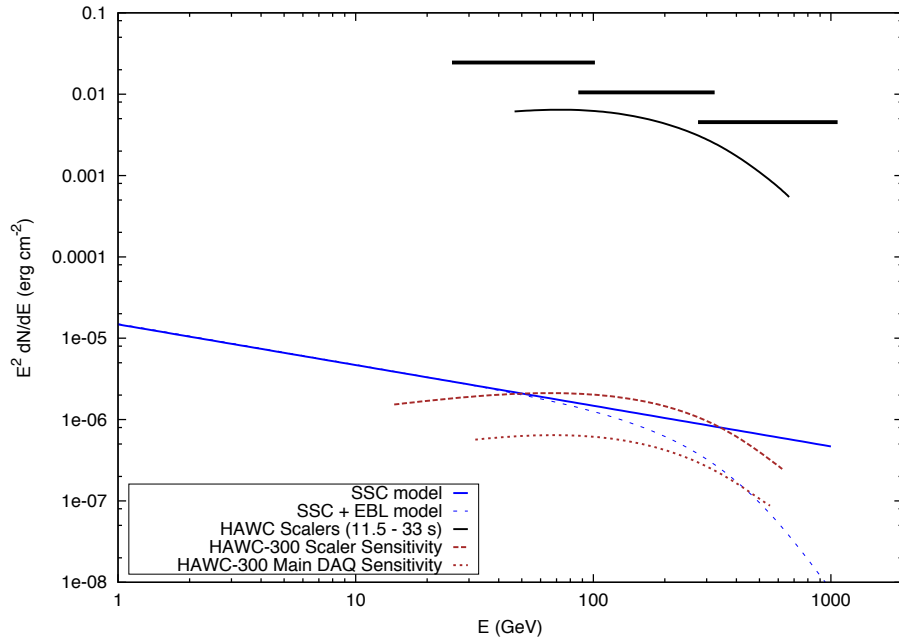

FIG. 4.— The SSC model proposed in this work and upper limits placed by the HAWC Observatory in the time interval [11.5 - 33 s]. Blue lines show the SSC model without (continuous) and with the effect of the EBL absorption (dashed). Black solid lines display the scaler limit. Brown dashed and dotted lines exhibit the sensitivity of the two HAWC DAQs for the full detector. (For details see Abeysekara et al. (2015)).